A Fast and Accurate Method for Glaucoma Screening from Smartphone-Captured Fundus Images

Yasmine Mrad, Yaroub Elloumi, Mohamed Akil, Mohamed Hédi Bedoui

A fast and accurate method for glaucoma screening from smartphone-captured fundus images

Yasmine Mrad[a] , Yaroub Elloumi[a,b,c] , Mohamed Akil[b] , Mohamed Hedi Bedoui[a]

[a]Medical Technology and Image Processing Laboratory, Faculty of medicine, University of Monastir, Tunisia.

[b]LIGM, Univ Gustave Eiffel, CNRS, ESIEE Paris, F-77454 Marne-la-Vallée, France.

[c]ISITCom Hammam-Sousse, University of Sousse, Tunisia.

HIGHLIGHTS

- Proposition of an accurate and fast method for glaucoma screening based on the vessel displacement
- Achievement of higher performance detection with smartphone captured fundus images
- Implementation of the method into a smartphone to provide a mobile aided screening system for glaucoma

GRAPHICAL ABSTARCT

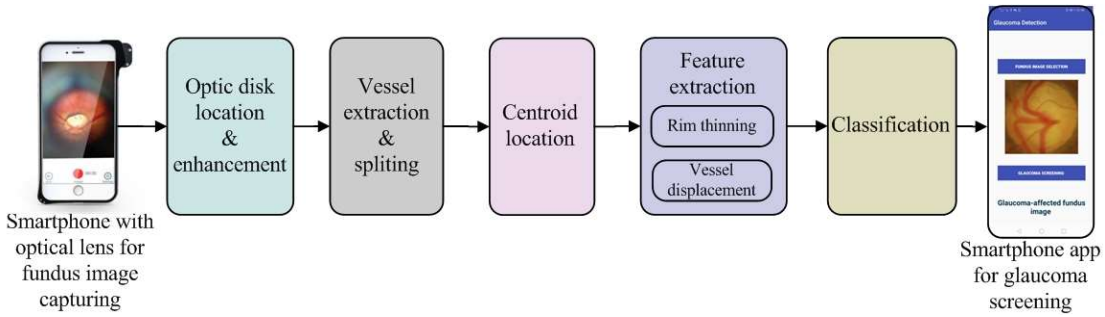

KEYWORDS

fundus image

glaucoma

feature extraction

classification

SVM

m-health

ABSTARCT

The glaucoma is an eye disease that causes blindness when it progresses in an advanced stage. Early glaucoma diagnosis is essential to prevent the vision loss. However, early detection is not covered due to the lack of ophthalmologists and the limited accessibility to retinal image capture devices.

In this paper, we present an automated method for glaucoma screening dedicated for Smartphone Captured Fundus Images (SCFIs). The implementation of the method into a smartphone associated to an optical lens for retina capturing leads to a mobile aided screening system for glaucoma. The challenge consists in insuring higher performance detection despite the moderate quality of SCFIs, with a reduced execution time to be adequate for the clinical use.

The main idea consists in deducing glaucoma based on the vessel displacement inside the Optic Disk (OD), where the vessel tree remains sufficiently modeled on SCFIs. Within this objective, our major contribution consists in: (1) segmenting retinal vessels inside the OD, (2) locating centroid points that adequately model the vessel distribution, (3) identifying features that relevantly reflect the vessel displacement, and (4) providing the feature set to a classifier in order to deduce the glaucoma disease. Furthermore, all processing steps are carefully chosen based on lower complexity, to be suitable for fast clinical screening.

A first evaluation of our method is performed using the two public DRISHTI-DB and DRIONS-DB databases, where 99% and 95% accuracy, 96.77% and 95.12% sensitivity and 100% and 94.73% specificity are respectively achieved. Thereafter, the method is evaluated using two fundus image databases respectively captured through a smartphone and retinograph for the same persons. We achieve 100% accuracy using both databases which assesses the robustness of our method. In addition, the detection is performed on 0.155±0.035 second when executed on a smartphone device. Our proposed smartphone app provides a cost-effective and widely accessible mobile platform for early screening of glaucoma in remote clinics or areas with limited access to fundus cameras and ophthalmologists.

This work was supported by the PHC-UTIQUE 19G1408 Research program.

1. Introduction

Glaucoma damages the Optic Nerve Head (ONH) due to elevated or inappropriate intraocular pressure in the eye. It is estimated that patients suffering from glaucoma will have reached 76 million by the end of 2020 and 111.8 million by 2040 [1]. Glaucoma gradually and asymptomatically causes the loss of the visual field [2]. It is often referred as a "silent thief of sight" which is noticed only when the disease progresses to a significant loss of peripheral vision. Therefore, the early diagnosis of glaucoma is essential to stop or slow the progression of the disease and to prevent blindness. Indeed, a delay is recorded in the glaucoma diagnosis due to several causes which are: (1) the lower ratio of ophthalmologists per population; (2) the high cost of glaucoma therapies which achieve 2,511$ and 803 € for advanced disease, respectively in United States and Europe [3]; and (3) the higher cost of the available clinical devices for retinal image capturing.

To facilitate access to early diagnosis, several studies have proposed automatic methods for glaucoma screening, which differ with respect to the glaucoma properties addressed for detection. Several methods such as the ones suggested in [4, 5, 6, 7, 8, 9, 10, 39, 28, 29, 33, 23] segmented the Optic Disk (OD) and the Optic Cup (OC) in order to deduce the Cup-to-Disc Ratio (CDR). Moreover, the segmented OD and OC were allowed to extract the Neuro-Retinal Rim (NRR) shape where glaucoma could be identified based on the ISNT rule [41]. Other methods have extracted the parapapillary atrophy which had an elliptical shape with the OD boundary having an intermediate intensity between the retina and the OD [42,43]. The related work of ONH location and OD/OC extraction were explicitly detailed in the review proposed by [31]. The blood vessels have been addressed in some work to screen glaucoma [11,12]. A strong correlation has been deduced between shape, location and density of vessels and the deterioration of the glaucomatous ONH, as studied in the survey put forward by Serhan et al. [41]. Indeed, some other methods have been based on detecting the Retinal Nerve Fiber Layer (RNFL) deterioration [13,14] which has been always deduced through vessel tree displacement outside the OD.

Those methods were dedicated for conventional retinography fundus images, which were characterized by a sharpness quality, as shown Fig.1(a). Accordingly, a high accurate segmentation of retinal components was ensured, and hence achieving efficient glaucoma screening. However, the capturing process required the presence of an ophthalmologist and the use of expensive conventional retinography devices.

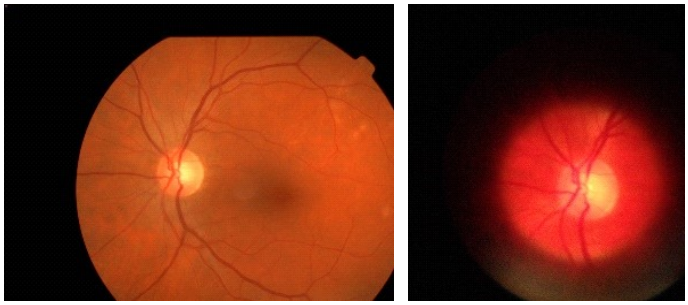

(a) (b)

Fig. 1.fundus images: (a) captured with retinograph; (b) captured with optical lens-associated smartphone

Furthermore, these detection methods used standard equipment that required the mobility of patients. As a result, these proposed methods did not address the problems leading to the delayed diagnosis of glaucoma. Moreover, few methods were addressed to reduce the execution time [35, 41], which presented a clinical constraint for employing the proposed methods.

Actually, several mobile devices for fundus image capturing have been suggested such as D-eye and iExaminer, which allow using smartphones in eye disease screening, taking advantage from their mobility, low-cost and high capabilities in terms of processing and storage [15, 16, 17]. It has been deduced that Smartphone Captured Fundus Images (SCFIs) have an acceptable quality compared to the images captured by ophthalmoscopes, where both fundus images, in Fig.1, are captured from the same eye using respectively a retinograph and an optical lens-associated smartphone. In [18], the D-eye showed considerable accuracy of CDR measurements compared to direct ophthalmoscopy. In addition, the D-eye gadget offered high performance for manually detecting fundus abnormalities compared to indirect ophthalmoscopy, with specificity of 0.97 and 0.98 for detecting the eye abnormalities and measuring the optic nerve size. Therefore, our main objective is to provide a Mobile Aided Screening (MAS) system for glaucoma. The challenges consist in ensuring higher accuracy detection and robustness with respect to the moderate quality of SCFIs, through a reduced execution time.

Indeed, the moderate quality of SCFIs involves a blurred and noised illustration of retinal components, as illustrated in Fig.1(b). Thus, the existing methods have fail to achieve accurate retinal component segmentation, and so an efficient glaucoma detection. Moreover, limited processing capacities of smartphones bring to expand the screening execution time, which is inadequate with respect to the clinical context. To avoid those problems, some work has been interested into proposing a mobile MAS system for glaucoma to achieve higher performance detection with lower processing complexity. The work proposed by [20] was indicated that the tele-glaucoma technology demonstrated moderate agreement on its ability to diagnose glaucoma and achieved 79% of specificity and 83% of sensitivity. The work described in [21] suggested a mobile application for glaucoma screening. The glaucoma detection was based on the CDR and the NRR thinning. Detection was ensured with accuracy of 0.7625 in 9.16 seconds, which was surpassed by several existing methods whether for efficiency or execution time. Recently, Martins and al [22] has propounded a method for diagnosing glaucoma dedicated for smartphone devices. Accuracy of 0.87, sensitivity of 0.85 and AUC of 0.93 were achieved under two seconds for retinograph-captured fundus images. However, the detection principle of all methods put forward in [20, 21, 22] was fully based on extracting the OD and the OC, where the segmentation performance might degrade in case of SCFIs. Indeed, no evaluation was performed using SCFIs or even with classical fundus images after data augmentation.

For this purpose, the objective of this work is to propose a novel method for glaucoma detection dedicated for SCFIs. The rest of the paper is expended to present the suggested method. The second section describes the automated method for glaucoma detection. The experimental evaluation of the

detection performance and the execution time is presented in section 3. The conclusion and some future work are detailed in section 4.

2. Fast and accurate method for glaucoma screening

2.1. Principle

Our challenges consist in proposing an accurate and robust method even with a moderate image quality. Furthermore, all processing steps are carefully chosen based on lower complexity, to be suitable for mobile implementation. At first, glaucoma damages the optic nerve where the main morphological changes occur inside the ONH. Indeed, glaucoma screening from the ONH brings to higher performance detection and low complexity processing [4, 5, 6, 7] in contrast to the methods exploring the whole retina, as synthetized in the comparative study performed in [41]. Moreover, SCFIs are characterized by a reduced filed of view against the classical fundus images, hence avoiding presenting the papillary atrophy located outside the ONH. Therefore, the first step of our method consists in locating the OD, as detailed in section 2.2.

Thereafter, we study the impact of glaucoma on the retinal components in order to identify the adequate ones for screening, taking into account the moderate quality of SCFIs. A healthy optic nerve corresponds to a tiny excavation. However, glaucoma damages the optic nerve fibers, thus expanding the excavation, as it can be deduced when comparing Fig.2(a) and Fig.2(c). Similarly, the OC appears with a reduced size in a healthy fundus image. For a glaucoma-affected one, the excavation growth leads to increase the OC size, while the OD size remains stationary, as respectively distinguished from the fundus images in Fig.2(b) and Fig.2(d). Elsewhere, the excavation growth does not occur similarly in all directions where the glaucoma leads to destroy the ISNT rule. With respect to this indication, several methods have segmented the OD and the OC to deduce whether the CDR or shape of the NRR to detect glaucoma.

In a healthy retina, vessels spread from the middle of the excavation, as shown in Fig.2(a). The vessels propagate beyond the large NRR, which appear with an equitable distribution in the OD, as modeled in Fig.2(b). Otherwise, the rise in the optic nerve fiber damage leads to join the vessel to the internal border of the excavation, as we can see in Fig.2(c). The perpendicular visual field to the retina leads to model vessels as shifted to the OD border, as depicted in Fig.2(d). Accordingly, the optic nerve fiber damage similarly affects the OC size and the vessel distribution, where both are able to reflect glaucoma severity. In

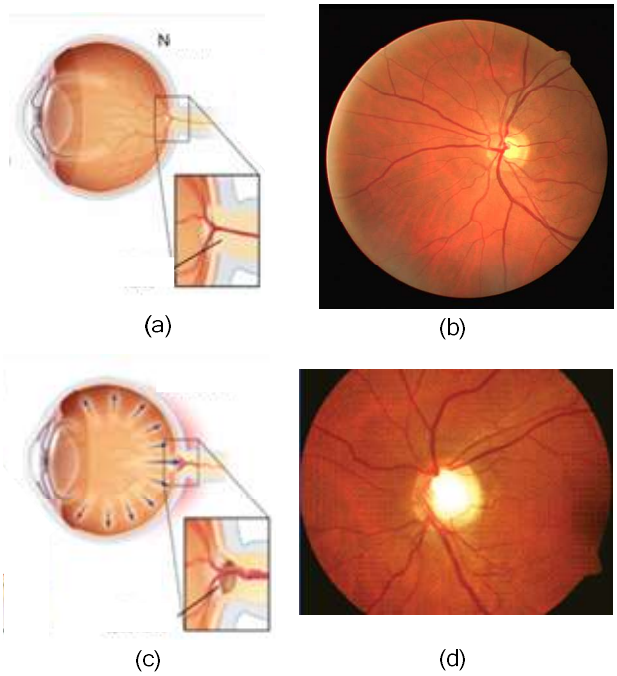

Fig. 2. (a) Optic nerve head excavation of healthy retina; (b) Fundus image of healthy retina; (c) Optic nerve head excavation of glaucomatous retina; (b) Fundus image of glaucomatous retina

the same vein, several methods have identified the glaucoma through segmenting and locating retinal vessels.

SCFIs are always blurred and noised due to the handheld aspect, which have a moderate quality with respect to classical images. Degradation principally affects the contrast of retinal components with respect to their neighborhood. However, the OD and the OC have close intensity and blurred borders, which leads to alter at once the OD and OC segmentation. By applying their ratio, such drop in performance considerably fakes glaucoma screening. In contrast, the vessel tree remains sufficiently represented in the OD. The vessel distribution is obviously distinguishable, despite the moderate quality.

For this purpose, the main idea of our method consists in screening glaucoma from SCFIs based on blood vessels. To guarantee the method robustness, our approach will be based on evaluating the distribution of the whole vessel tree rather than based on each vessel separately. Therefore, the vessel tree is segmented and partitioned into quadrants with respect to the ISNT notion, as described respectively in sections 2.3 and 2.4. Then, a position marker of vessel distribution on each quadrant is located, which called centroid. After that, a feature set is

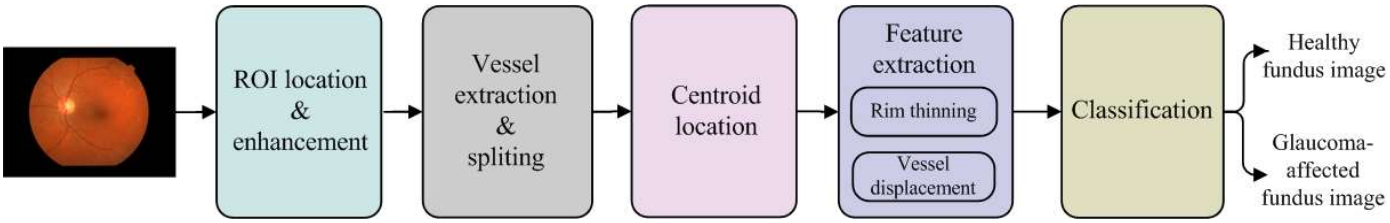

Fig. 3. Flowchart of proposed method for glaucoma screening

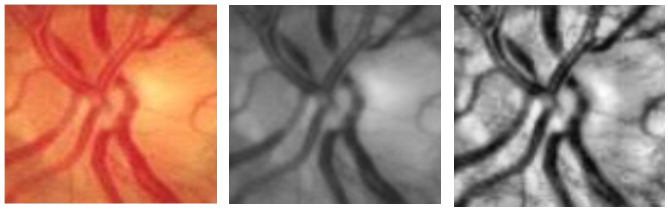

(a) (b) (c)

Fig. 4. (a) Healthy OD; (b) Green channel, (c) OD after applying CLAHE algorithm

extracted and provided to a classifier to deduce glaucoma, as summarized in the method flowchart in Fig.3.

2.2. OD extraction and enhancement

The method proposed in [44] ensured locating the ONH based on circularity and intensity through applying the radon transform. The method achieved higher accurate performance among the existing methods [31, 34], where 100% accuracy was performed to locate the ONH in the public DRIVE database. We note that this method can be configured to locate a sub-image having the same OD size. Afterwards, this method was extended to provide a mobile computer aided system for ONH detection [24]. Processing was optimized to reduce complexity, where the same detection accuracy was performed a in reduced time when executed in a smartphone device. Therefore, the method suggested in [24] would be implemented, which extracted the OD sub-images.

In addition, glaucoma screening requires detecting overlapped retinal components. However, SCFIs are characterized by a non-balanced contrast, which result in failed detection. Consequently, the second step leads to enhance the sub-image contrast with respect to the blood vessels. We proceed to extract the green channel which reveals a better contrast between the retinal structures. Next, the CLAHE algorithm is applied to ensure a better contrast equalization into the ONH region, where the results of each step are illustrated in Fig.4.

2.3. Vessel segmentation and splitting

we proceed to segment the vessel tree into the located OD. The first step consists in inversing the OD brightness in order to model the blood vessel with higher intensity. Within this objective, the "black-hat" morphological operator is applied where the result is depicted in Fig.5(b). Then, the Otsu technique is applied to distinguish vessel from the OD background [30]. Finally, the "Medianblur" filter is used to reduce noise, which can be caused by small blood lesions [27], as shown in Fig.5(c).

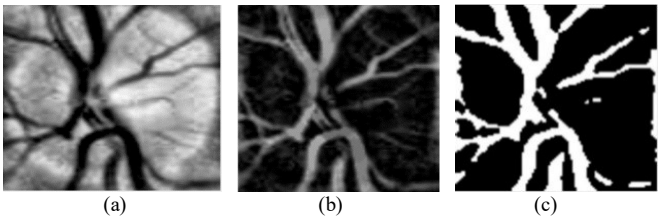

(a) (b) (c)

Fig. 5. Blood vessel Segmentation :(a) Green channel, (b) Black-Hat inversion, (c) Otsu segmentation

The vessel tree displacement caused by glaucoma is developed mainly in superior, inferior and nasal quadrants, where the temporal quadrant contains less vessels than the other ones [11,46]. Thereby, vessels should be partitioned on their quadrants to deduce the glaucoma displacement. Within this objective, we proceed to split the segmented vessels into four quadrants through superimposing four different masks, illustrated in Fig.6(a)-Fig.6(d), to the OD where the results are respectively depicted in Fig.6(e)-Fig.6(h).

2.4. Centroid location

It is essential to define a parameter that can reflect vessel displacement into quadrants. Our main idea consists in computing a centroid reference point for vessels belonging to the same quadrant. Then, glaucoma is deduced based on the centroid remoteness. We note that the vessel centroid is figured out in terms of all positions of vessel pixels. Hence, a blurred vessel tree has a marginal impact when extracting centroid position.

The method put forward by [11] first identified elementary centroid of each pixel cluster. Then, clusters are fused and their centroids are updated until grouping all clusters having a single centroid. In order to reduce processing complexity, we propose a novel approach to locate the centroids. First, for the vessel pixels of each quadrant, the sum of their horizontal coordinate Q_x and vertical coordinate Q_y are computed, as indicated respectively in equations 2 and 3. The centroid horizontal coordinate C_x (resp. vertical coordinate C_y) corresponds to the ratio between Q_x (resp. Q_y) and the number of vessel pixels N_{VP}, as indicated in equations 4 (resp. in equation 5).

$$N_{VP} = \sum_{0}^{\text{nbc}} \sum_{0}^{\text{nbr}} I_{vessel}(x_v, y_v) \quad (1)$$

$$Q_x = \sum_{1}^{N_{VP}} x_v \quad (2)$$

$$Q_y = \sum_{1}^{N_{VP}} x_v \quad (3)$$

$$C_x = \frac{Q_x}{N_{VP}} \quad (4)$$

$$C_y = \frac{Q_y}{N_{VP}} \quad (5)$$

where $I_{vessel}(x_v, y_v) = (255, 255, 255)$. For example, Fig.7(a) and Fig.7(b) illustrate the centroid locations in respectively healthy and glaucoma ODs, respectively.

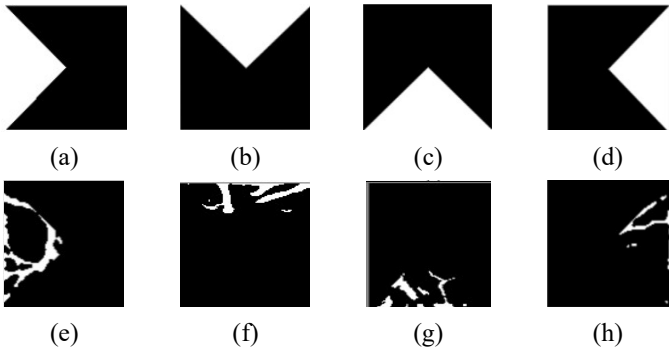

(a) (b) (c) (d)

(e) (f) (g) (h)

Fig. 6. (a-d): Masks used for quadrant partition; (e-h): blood vessels of each quadrant

2.5. Feature extraction

2.5.1. Neuro-retinal rim thinning

In a healthy fundus image, the rim has a large board through the OD. The glaucoma involves increasing the OC and hence reducing the NRR. This criterion remains very helpful for clinical staff to diagnose glaucoma [31]. Within this context, the method described in [49] computed the rim-to-disc ratio in order to deduce glaucoma. In [46], the rim area of each quadrant is figured out in order to compute a ratio that reflects glaucoma.

In fact, a significant correlation is distinguished between the blood vessel distribution into quadrants and the NRR lost [45]. In a healthy fundus image, the reduced size of excavation leads to merging blood vessels to the OD center. Consequently, centroids appear as clustered in the OD middle region. The excavation growth caused by glaucoma shifts blood vessels away from the OD center until getting closer to the OD borders [11,12], such as the difference between fundus images in Fig.2(b) and Fig.2(d). With respect to the excavation growth, the centroid positions become spaced.

Subsequently, we aim to provide features that reflect the centroid remoteness. Since the four zones are affected on both extremities of the perpendicular axis, we quantify the centroid remoteness through Euclidian distances between each neighbor centroid. The temporal centroid escapes to a similar shifting since it contains less vessels. Therefore, we choose to overpass the temporal quadrant in order to guarantee higher accuracy detection. Accordingly, we consider two features which correspond to the distances between superior-nasal and inferior-nasal centroids, as illustrated with red arrows in Fig.7, where the distances in the healthy OD in Fig.7(a) appear clearly smaller than the ones in the glaucoma-affected OD in Fig.7(b).

2.5.2. Vessel displacement in relation to the ISNT rule

In a healthy OD, the inferior quadrant contains the thickest rim, followed by the superior, nasal and temporal quadrants, as known as the ISNT rule [47]. Similarly, inferior and superior quadrants include the wide portion of the vessel tree [46]. For a glaucoma-affected fundus image, the optic nerve excavation growth leads to expand the OC. The rim thinning does not occur similarly in all directions where rim thicknesses into quadrants changes differently. The glaucoma involves violating the ISNT rule where the excavation expands principally in the inferior and superior quadrants. As a result, the thinning leads to shift the blood vessels from inferior and superior regions towards the nasal region [46]. Consequently, the centroids of inferior and superior quadrants remain closed to the OD border.

In contrast, the added vessels to the nasal quadrant arise from inferior, superior and temporal neighborhood quadrants. The shifted vessels significantly affect the distribution of vessel density, and so the nasal centroid location. Hence, even with a thinned rim, the nasal centroid is not always relocated to be near of OD border. Similarly, the reduced vessel density in a temporal quadrant and the vessel displacement in the direction of the OD center do not allow modeling the temporal centroid displacement in terms of glaucoma. Accordingly, we extract two features that reflect the ISNT, which correspond to two Euclidian distances between inferior and superior centroids and their corresponding borders, as indicated with blue arrows in both images of Fig.7.

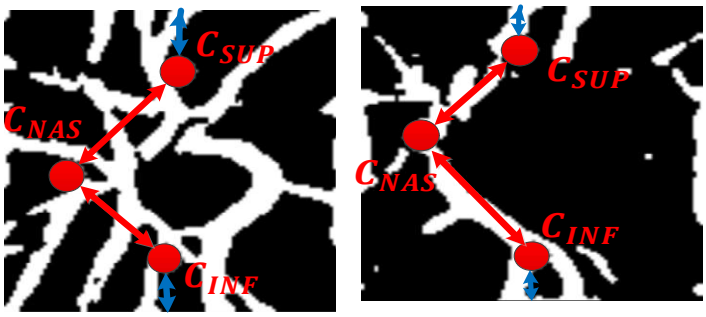

(a) (b)

Fig. 7. Centroids of blood vessels located in different zones of OD: (a) Healthy OD, (b) Glaucoma affected OD

2.6. Classifier

The Support Vector Machine (SVM) classifier is a supervised learning method, used in classification and regression problems. It attempts to fit a hyperplane through the feature space in order to discriminate between classes provided as grountruth data on the training process. The SVM classifier is frequently employed for the pathology detection method, especially for binary classification, which achieves higher performance detection. This higher accuracy is ensured even with a reduced training dataset. Moreover, the SVM classifier is characterized by lower complexity whatever the dataset size is. For this purpose, we choose the SVM as a classifier on our proposed method.

The kernel function is used to map the feature points to a higher dimension [36]. Since features are not linearly separable, the RBF kernel is employed, which is chosen based on the accuracy and the execution time. Elsewhere, the SVM is used with a gamma value equal to 0.1 and a C value equal to 1, where the values are experimentally chosen based on detection performance.

3. Experimental results

3.1. Evaluation of glaucoma screening method

3.1.1. Dataset and evaluation metrics

To test and evaluate the proposed method, two publically available datasets are selected which are frequently used in serval methods for glaucoma assessment. The first one is the DRISHTI-DB dataset which contains a total of 101 images provided by the Medical Image Processing (MIP) group, IIIT Hyderabad. All images were taken with dilated eyes, centered on the OD with a field of view of 30 degrees and a dimension of 2896×1944 pixels. The second dataset is the DRIONS-DB [53-55] which contains 110 digital retinal images including 50 normal images and 60 glaucoma images with a dimension of 600 × 400 pixels. The fundus images were acquired from patients approximately 53 years of age, approximately centered on the ONH [54]. We note that DRIONS-DB contains suspect fundus images which are avoided in our experimentation. The overall healthy and glaucoma-affected images are mentioned in Table1.

Table 1. Databases used in proposed method

Database	Number of fundus images	
	Healthy	Glaucoma images
DRIONS-DB	40	20
DRISHTI-GS	31	70

The performance of our method is evaluated through the accuracy, sensitivity and specificity metrics [56, 57], which are computed as indicated in equations 6, 7 and 8.

$$\text{Sensitivity} = \frac{\text{TP}}{\text{TP} + \text{FN}} (6)$$

$$Specificity = \frac{TN}{TN + FP} (7)$$

$$\text{Accuracy} = \frac{\text{TP} + \text{TN}}{\text{TP} + \text{FP} + \text{TN} + \text{FN}} (8)$$

where TP (True Positive) is the number of images classified correctly as glaucoma-affected, TN (True Negative) is the number of images classified correctly as healthy, FP (False Positive) is the number of healthy images identified as glaucomatous and FN (False Negative) is the number of glaucoma-affected images classified as healthy. To correctly evaluate our contribution, those metrics are computed after locating the OD using the method detailed in [24].

3.1.2. Performance evaluation of glaucoma screening method

This method is evaluated using each dataset separately, where all fundus images are used for training and testing steps. The experimentation shows that our method achieves 98.01% accuracy, 93.54% sensitivity and 100% specificity when the evaluation is performed using the DRISHTI-DB database. Furthermore, when the evaluation is performed using DRIONS-DB database, our proposed method provides 95% of accuracy, 95.12 % of sensitivity and 94.73% of specificity, as shown in Table 2. Accordingly, the higher detection performance on both datasets confirms the accuracy of our suggested method for glaucoma screening.

Table 2. Performance of the proposed method

DB	Accuracy	Sensitivity	Specificity
DRISHTI-DB	99%	96.77%	100%
DRIONS-DB	95%	95.12%	94.73%

As the DRISHTI-DB is widely used for evaluating several automated methods of glaucoma screening, we compare our method with recent ones where accuracy, sensitivity and specificity are depicted in Table 3. It is obviously distinguished that our method outperforms several existing state-of-the-art glaucoma detection methods, and is tabled among the most highly performant ones.

Table 3. Performance comparison with state-of-the-art methods

Method	Accuracy	Sensitivity	Specificity
[58]	82.20%	--	--
[59]	--	95,52%	--
[60]	76.77%	--	--
[61]	95%	100%	90%
[57]	98%	100%	94.4%
Proposed method	**99%**	**96.77%**	**100%**

3.2. Performance evaluation with respect to SCFIs

3.2.1. Dataset

The second experimentation consists in evaluating the suggested method using SCFIs. Within this objective, we evaluate our method using the RIAMP dataset proposed in [62], which contains healthy and glaucoma-affected fundus images acquired from 16 people. For each person, a first fundus image was captured with Topcon retinal camera and three others with the optical lens "iExaminer" snapped to a smartphone iPhone 4S. For instance, fundus images captured form healthy and

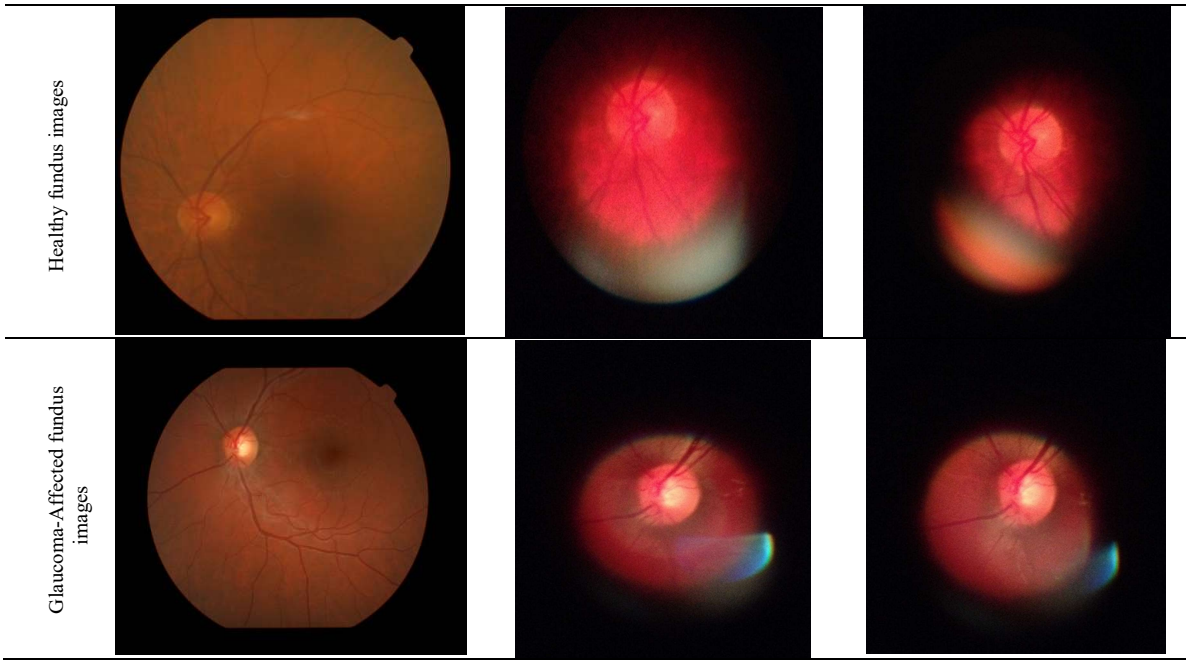

Fig. 8. Fundus images: (a) captured with Topcon retinal camera; (b) captured with iExaminer

glaucomatous retinas are shown respectively in first and second lines of Fig.8. This dataset allows demonstrating that images acquired by mobile phones are applicable for the automatic detection of the OD and the OC.

The classical fundus images are provided to an ophthalmologist to generate the groundtruth. Some retinas are considered as suspect, whether for classical or smartphone captured fundus images, which requires additional diagnosis to deduce if the patient is glaucoma-affected. Therefore, suspect images are avoided to keep only healthy and glaucoma-affected ones, which correspond respectively to two and nine people, for both classical and SCFI databases.

We notice that three smartphone captured fundus images are acquired for each person. Therefore, to have a stability between classes and achieve a sufficient dataset size for training, two images for each glaucoma-affected person are identified and added, based on their better quality. The structure of both datasets are detailed in Table 4.

Table 4. Selected images from RIAMP database

	Healthy images	Glaucoma images
Standard images	9	2
Mobile images	9	4

3.2.2. Performance evaluation

To evaluate the robustness of our method, the experimentation consists in evaluating our method using each dataset separately and then comparing the achieved detection performance. For each dataset, the training and testing processes are performed using the same image set. Thereafter, the metrics of accuracy, sensitivity and specificity are computed to evaluate the method for each dataset, which are depicted in Table 5.

Table 5. Detection performances of our method in terms of datasets

	Accuracy	Sensitivity	Specificity
Standard images	100%	100%	100%
Mobile images	100%	100%	100%

Based on the experimental results, we distinguish that our proposed method correctly detects all fundus images. Furthermore, the same detection performance is ensured even with smartphone captured fundus images. Accordingly, this experiment proves the robustness of the suggested method with respect to the moderate quality caused by the mobile device capturing. Hence, we can deduce that our method is adequate to be implemented it on a MAS system for glaucoma.

3.3. MAS system for glaucoma as smartphone app

The whole method is implemented as an app on an android operating system through the android SDK. This latter is a software development kit which provides several functions to fully use the system architecture and components. All image processing and machine learning steps are implemented using the "Open Source Computer Vision (OpenCV)" library [37, 67]. This library has more than 2,500 optimized algorithms, which includes a comprehensive set of both classic and state-of-the-art computer vision and machine learning algorithms. It is developed using C++ and can be supported by several operating systems and interfaced through many languages such as Python, JAVA and MATLAB. The OpenCV functions are implemented on an Android app using the Android Native Development Kit (NDK) [38], which allows compiling native application codes such as C/C ++ for Android applications to run on the Dalvik virtual machine. With this method, native codes can be used repeatedly and the execution speed can be faster. The Android NDK provides the native API compiler system and packages the native codes into APKs by integrating JAVA Native Interface (JNI) [68]. A graphical use interface is developed where the first step consists at uploading a fundus images from the gallery through the button entitled "Fundus image selection". Thereafter, the whole method is run through a button called "glaucoma detection". The detection result is displayed below the button indicating the provided class, as shown in Fig.9.

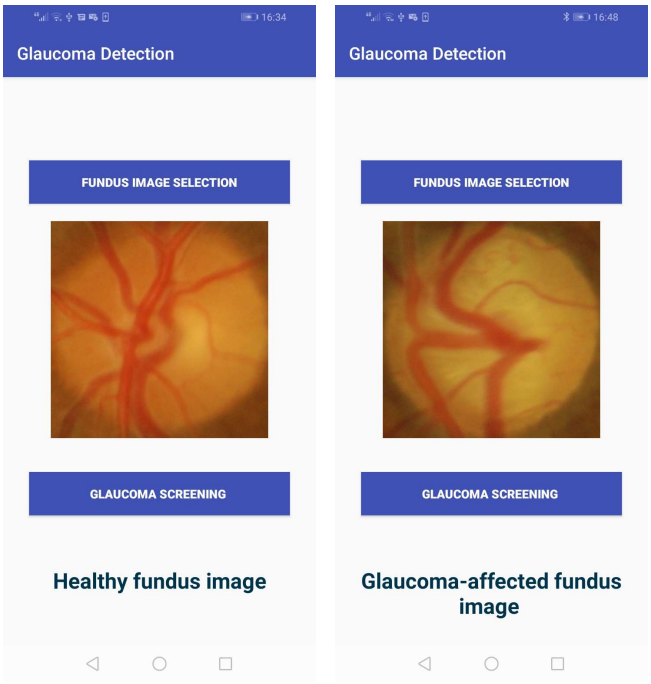

Fig. 9. Graphical Use Interfaces of the application

3.4. Computational performance of MAS system

3.4.1. Computational performance analysis

The CLAHE algorithm spreads all pixels to adjust pixel values, where the processing complexity is about $(n \times n)$ [69], where $(n \times n)$ is the OD sub-image size. The Black-hat filter inverses pixel values. Therefore, each processing requires $(n \times n)$ and the Otsu thresholding tests each value is order to assign 0 or 255, where each processing requires $(n \times n)$ to be done [70, 71]. Next, the Median Blur is processed for each pixel to remove noise, which is performed in $(n \times n)$ instructions. Four masks are applied to the provided image, where each one requires $(n \times n)$. After that, the processing of locating each centroid leads to adding all pixel coordinates, and so is performed in $(n \times n)$. Finally, the classification ensured by the SVM classifier is equal to $\max((f \times d), d^2)$ [72], where f is the number of features and d is the image number used for training, hence requiring constant computational complexity. As a consequence, the whole method requires the complexity of $O(n \times n)$ to be done.

3.4.2. *Execution time evaluation*

In this section, we evaluate the execution time of our method when implemented in the smartphone as an app. For this purpose, we quantify the execution times of glaucoma screening for SCFIs indicated in Table 7, where their values are depicted in Fig.10. We note that the architectural characteristics mentioned in the last line of Table 8. It is deduced that the average execution time is equal to 0.155±0.035 second, where the difference is registered whether for healthy or glaucoma affected images. The achieved execution times are perfectly adequate with the clinical context for ensuring glaucoma screening.

Thereafter, we compare our method to the state-of-the art ones where the execution times and hardware and software tools are respectively mentioned in the second, third and fourth columns of Table 8. As mentioned in the introduction, several methods do not focus on computational performance with execution times above 10 seconds in several methods. Furthermore, our smartphone-based method ensures the faster glaucoma screening, jointly with the method proposed in [66] which is performed in a desktop architecture having a processor with a 3Ghz of frequency. Among methods aiming for mobile glaucoma screening, our app outperforms the work proposed [22] in terms of detection performance and execution time where glaucoma is deduced under tow seconds with 0.87 accuracy and 0.85 sensitivity.

4. Conclusion

In this paper, we have put forward a method for glaucoma screening dedicated to SCFIs. The method principle consists in identifying the main glaucoma proprieties that rely in the OD, reflecting proprieties through carefully selected features and providing them to a supervised classifier. Our method achieves detection with 99% accuracy, 96.77% sensitivity, and 100% specificity when evaluated using the DRISHTI-DB. The method implementation through an app leads to a mobile computer-aided system for glaucoma detection. The experimentation confirms that our method ensures performant detection even when using SCFI. Besides, the glaucoma screening is performed on 0.155 second which is adequate for clinical issues.

In future work, we aim to extend our method in order to provide the severity stage of glaucoma screening. In addition, other ocular pathologies can be detected such as diabetic retinopathy and age macular degeneration. Moreover, the smartphone app can ensure uploading the fundus images to be transferred to ophthalmologists to anticipate medical care and therapy.

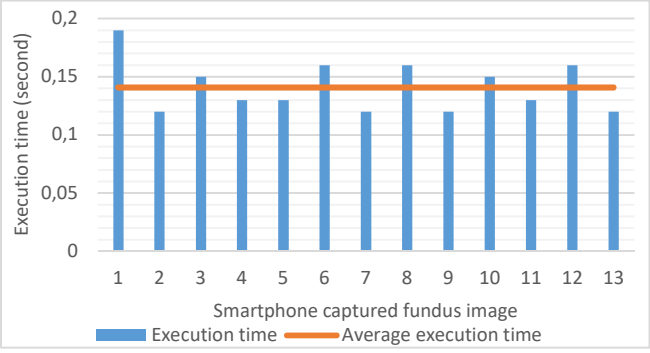

Fig. 10. Execution times in terms of smartphone captured fundus images

Table 8. Execution times in terms of hardware and software tools of glaucoma detection methods

Glaucoma detection methods	Execution time (in seconds)	Hardware tools	Software tools
[14]	25	core i7, 3.4 GHz RAM : 4GB	MATLAB
[59]	19.44	Intel core i7, 3.40 GHz	MATLAB
[64]	18	Intel Core i3, 3.5 GHz RAM: 6GB	Python 2.7 & OpenCV 2.4
[57]	11	Intel Xeon, 3.3 GHz, RAM : 8 GB	Python environment with Anaconda
[21]	9.16±0.78	Cloud platform	- -
[63]	8.1	quad core, 2.66 GHz	MATLAB
[65]	2.4	Processor : NVIDIA Tesla P40 GPU	Python based on Keras with Tensorflow backend
[22]	< 2	Samsung S8, Quad core, Up to 2.3GHz,	Python & TensorFlow Lite
[66]	from 0.12 to 0.17	dual core, 3.0 GHz, RAM : 3 GB	--
Proposed method	**0.155±0.035**	Quad-core, 1.4GHz, ARM cortex- A53 RAM : 2GO	Android 8.1 & OpenCV 3.5

Acknowledgements

Funding for this study came from Campus-France through the PHC-UTIQUE Research program (grant number: 19G1408). The authors acknowledge the help of Dr. Aymen Daldoul, ophthalmologist in the hospital center of Nevers agglomeration (France), to provide the groundtruth of smartphone-captured fundus images.

REFERENCES

[1] Maheshwari S, Pachori R B, Acharya R. Automated Diagnosis of Glaucoma Using Empirical Wavelet Transform and Correntropy Features Extracted From Fundus Images. IEEE Journal of Biomedical and Health Informatics 2016;21:803–813.

[2] Hagiwara Y, Koh JEW, Tan JH, Bhandary SV, Laude A, Ciaccio EJ, et al. Computer-aided diagnosis of glaucoma using fundus images: A review. Computer Methods and Programs in Biomedicine 2018;165:1–12. https://doi.org/10.1016/j.cmpb.2018.07.012

[3] Poemen P, Emmy Y, Clement C T .US Ophthalmic Review. VOLUME 7 ISSUE 2 - FALL 2014

[4] Soorya M, Issac A, Dutta MK. An automated and robust image processing algorithm for glaucoma diagnosis from fundus images using novel blood vessel tracking and bend point detection. International Journal of Medical Informatics 2018;110:52–70.

[5] Cheng, J, Yin F, Wong, DWK, Tao D, Liu. Sparse Dissimilarity-Constrained Coding for Glaucoma Screening. IEEE Transactions on Biomedical Engineering 2015;62:1395–1403.

[6] Cheng J, Liu J, Xu Y, Yin F, Wong DWK , Tan NM, Tao D, et al. Superpixel Classification Based Optic Disc and Optic Cup Segmentation for Glaucoma Screening. IEEE Transactions on medical imaging 2013;32:1019 - 1032

[7] Yin F, Liu J, Wong DWK, Tan NM, Cheung C, Baskaran M, et al .Automated Segmentation of Optic Disc and Optic Cup in Fundus Images for Glaucoma Diagnosis. In: 2012 25th IEEE International Symposium on Computer-Based Medical Systems (CBMS); 2012.

[8] Khalil T, Akram MU, Khalid S, Jameel A .Improved automated detection of glaucoma from fundus image using hybrid structural and textural features .IET Image Processing 2017;11: 693 - 700

[9] Bock R, Meier J, Nyúl LG, Hornegger J, Michelson G. Glaucoma risk index:Automated glaucoma detection from color fundus images. Medical Image Analysis 2010; 14(3):471–481.

[10] Krishnan MMR, Faust O. Automated glaucoma detection using hybrid feature extraction in retinal fundus images. Journal of Mechanics in Medicine and Biology 2013; 13 (1):1350011-1350032.

[11] Fuente-Arriaga JA, Felipe-Riverón EM, Garduño-Calderón E. Application of vascular bundle displacement in the optic disc for glaucoma detection using fundus images. Computers in Biology and Medicine 2014; 47(1).27–35.

[12] Nayak J, Acharya UR, Bhat PS, Shetty N, Lim TC. Automated diagnosis of glaucoma using digital fundus images. Journal of Medical Systems 2009; 33(5):337-46.

[13] Lamani D. Early detection of glaucoma through retinal nerve fiber layer analysis using fractal dimension and texture feature. International Journal of Research in Engineering and Technology . 2014;03:158–163.

[14] Panda R,Puhan NB,Rao A,Padhy D, Panda G. Automated retinal nerve fiber layer defect detection using fundus imaging in glaucoma. Comput Med Imaging Graph. 2018;66:56–65.

[15] Mercado C, Welling J, Oliva M, Li J ,Gurung R, Ruit S, et al. Clinical Application of a Smartphone-Based Ophthalmic Camera Adapter in Under-Resourced Settings in Nepal. Journal of Mobile Technology in Medicine .2017;6, 34–42.

[16] Sharma A. Emerging Simplified Retinal Imaging. Dev Ophthalmol. 2017;60, 56–62.

[17] Akil M, Elloumi Y. Detection of retinal abnormalities using smartphone-captured fundus images: a survey. Real-Time Image Processing and Deep Learning 2019; 21

[18] Dickson D, Jain SF. MacDonald C, Song H, Agraz D, Morgan L, et al. Comparison Study of Funduscopic Exam of Pediatric Patients Using the D-EYE Method and Conventional Indirect Ophthalmoscopic Methods. Open Journal of Ophthalmology 2017;07(03):145-152

[19] Akram, MU, Tariq A, Khalid S, Javed MY, Abbas S,Yasin UU .Glaucoma detection using novel optic disc localization hybrid feature set and classification techniques. Australasian Physical & Engineering Sciences in Medicine 2015;38:643–655

[20] Thomas SM, Jeyaraman MM., Jeyaraman M, Hodge WG, Hutnik CML,Costella J,Malvankar-Mehta MS. The effectiveness of teleglaucoma versus in-patient examination for glaucoma screening: a systematic review and meta-analysis. PLoS ONE 9 2014;9(12):e113779

[21] Guo F, Mai Y, Zhao X, Duan X, Fan Z,Zou B, Xie B. A Mobile App Using the Measurement of Clinical Parameters for Glaucoma Screening. IEEE Access 2018; PP(99):1-1

[22] Martins J, Cardoso JS, Soares F. Offline computer-aided diagnosis for Glaucoma detection using fundus images targeted at mobile devices. In Computer Methods and Programs in Biomedicine 2020;192:105341

[23] Balakrishnan U. An automatic segmentation of optic disc and cup region from medical images for glaucoma detection .Journal of Innovative Optical Health Sciences 2017;10(6):

[24] Elloumi Y, Akil M, Kehtarnavaz N. Mobile computer aided system for optic nerve head detection. Computer Methods and Programs in Biomedicine (CMPB) 2018;162:139-148

[25] Zilly J, Buhmann JM, Mahapatra, D. Glaucoma detection using entropy sampling and ensemble learning for automatic optic cup and disc segmentation. Computerized Med. Imaging 1470 and Graphics 2017;55 , 28–41.

[26] Issac A, Sarathi MP, Dutta MK.An adaptive threshold based image processing technique for improved glaucoma detection and classification. Computer Methods and Progr in Biomedicine 2015 ;122 :229–244

[27] Zhu Y, Huang C. An Improved Median Filtering Algorithm for Image Noise Reduction.In: 2011 Third International Conference on Measuring Technology and Mechatronics Automation, April 1-2 2012, Macao 25, 609–616.

[28] Joshi GD,Sivaswamy J,Krishnadas SR. Optic Disk and Cup Segmentation From Monocular Color Retinal Images for Glaucoma Assessment. IEEE transactions on medical imaging 2011;30(6):1192–205.

[29] Abdullah M., Fraz MM, Barman SA. Localization and segmentation of optic disc in retinal images using circular Hough transform and grow-cut algorithm. PeerJ 2016; 4:e2003.

[30] Muramatsu C, Nakagawa T, Sawada A, Hatanaka Y, Hara T, Yamamoto T, et al. Automated segmentation of optic disc region on retinal fundus photographs. Computer Methods Programs Biomedicine 2011;101(1):23-32

[31] Haleem SM, Han L, Hemert JV, and Li B. Automatic extraction of retinal features from colour retinal images for glaucoma diagnosis: a review. Comput Med Imaging Graph 2013; 37(7-8):581-96.

[32] Abbas Q. Glaucoma-Deep: Detection of Glaucoma Eye Disease on Retinal Fundus Images using Deep Learning. International Journal of Advanced Computer Science and Applications 2017;8(6)

[33] Al-Bander B , Williams BM, Al-Nuaimy W, Al-Taee M, Pratt H , Zheng Y. Dense Fully Convolutional Segmentation of the Optic Disc and Cup in Colour Fundus for Glaucoma Diagnosis. Symmetry 2018; 10(4):87

[34] Akil M, Sayadia S, Elloumi Y, Bedoui MH. Computational efficiency of optic disk detection on fundus image: a survey. In: Real-Time Image and Video Processing 2018;15. https://doi.org/10.1117/12.2304941

[35] Elloumi Y, Akil M, Boudegga H.Ocular diseases diagnosis in fundus images using a deep learning: approaches, tools and performance evaluation.In : Real-Time Image Processing and Deep Learning 2019

[36] Acharya UR, Ng EYK, Eugene LWJ, Noronha KP, Min LC, Nayak KP, Bhandary SV.Decision support system for the glaucoma using Gabor transformation. Biomedical Signal Processing and Control 2015:15;18–26. https://doi.org/10.1016/j.bspc.2014.09.004

[37] Domínguez C, Heras J, Pascual V.IJ-OpenCV: Combining ImageJ and OpenCV for processing images in biomedicine.. Computers in biology and medicine 2017; 84; 189–194. https://doi.org/10.1016/j.compbiomed.2017.03.027

[38] Tedeschi A, Benedetto F. A real-time automatic pavement crack and pothole recognition system for mobile Android-based devices. Advanced Engineering Informatics 2017; 32:11–25. DOI : https://doi.org/10.1016/j.aei.2016.12.004

[39] Zilly J, Buhmann, JM, Mahapatra D. Glaucoma detection using entropy sampling and ensemble learning for automatic optic cup and disc segmentation. Computerized Med Imaging Graph 2017;55:28–41. https://doi.org/10.1016/j.compmedimag.2016.07.012

[40] Mvoulana A, Kachouri R, Akil M. Fully automated method for glaucoma screening using robust optic nerve head detection and unsupervised segmentation based cup-to-disc ratio computation in retinal fundus images.Computerized Medical Imaging and Graphics 2019;77, 101643. https://doi.org/10.1016/j.compmedimag.2019.101643

[41] Sarhan A, Rokne J, Alhajj R.Glaucoma detection using image processing techniques: A literature review . Computerized Medical Imaging and Graphics , 2019;78:101657. https://doi.org/10.1016/j.compmedimag.2019.101657

[42] Muramatsu C, Nakagawa T, Sawada A, Hatanaka Y, Hara T, Yamamoto T, et al. Automated segmentation of optic disc region on retinal fundus photographs: Comparison ofcontour modeling and pixel classification methods. IEEE Transactions on Medical Imaging 2011;101:23–32.

[43] Tan N, Liu J, Lim J, Zhang Z, Lu S, Li H, et al. Automatic detection of pathological myopia using variational level set. In: 31st Annual International Conference of the IEEE Engineering in Medicine and Biology Society;2009:3609–12.

[44] Pourreza-Shahri R, Tavakoli M, Kehtarnavaz N. Computationally efficient optic nerve head detection in retinal fundus images. Biomedical Signal Processing and Control 2014;11:63–73. https://doi.org/10.1016/j.bspc.2014.02.011

[45] Radcliffe NM, Smith SD, Syed ZA, Park SC, Ehrlich JR, De Moraes CG, Liebmann JM, Ritch R. Retinal Blood Vessel Positional Shifts and Glaucoma Progression. Ophthalmology 2014; 121:842–848. https://doi.org/10.1016/j.ophtha.2013.11.002

[46] Issac A, Sarathi M, Dutta M. An Adaptive Threshold Based Image Processing Technique for Improved Glaucoma Detection & Classification.

Computer methods and programs in biomedicine 2015; 122. https://doi.org/10.1016/j.cmpb.2015.08.002

[47]Jonas JB, Fernández MC, Stürmer J. Pattern of Glaucomatous Neuroretinal Rim Loss. Ophthalmology 1993;100:63–68. https://doi.org/10.1016/S0161-6420(13)31694-7

[48] Harizman N, Oliveira C, Chiang A., Tello C, Marmor M, Ritch R , et al . The ISNT rule and differentiation of normal from glaucomatous eyes. Archives of ophthalmology 2006;124:1579–1583. https://doi.org/10.1001/archopht.124.11.1579

[49] Akram, M, Tariq A, Khalid S, Javed M, Abbas S, Yasin U. Glaucoma detection using novel optic disc localization, hybrid feature set and classification techniques. Australasian Physical & Engineering Sciences in Medicine 2015;38:643–655. https://doi.org/10.1007/s13246-015-0377-y

[50] Sivaswamy J, Krishnadas S, Chakravarty A, Joshi G, Ujjwal.A Comprehensive Retinal Image Dataset for the Assessment of Glaucoma from the Optic Nerve Head Analysis.JSM Biomedical Imaging Data Papers 2015;2(.1):1004.

[51] Carmona EJ, Rincón M, García-Feijoó J, Martínez-de-la-Casa JM. Identification of the optic nerve head with genetic algorithms," Artificial Intelligence in Medicine 2008;43(3):243-59. https://doi.org/10.1016/j.artmed.2008.04.005

[52] Sivaswamy J, Krishnadas SR., Datt Joshi G, Jain M, Syed Tabish AU. Drishti-GS: Retinal image dataset for optic nerve head(ONH) segmentation, In: 2014 IEEE 11th International Symposium on Biomedical Imaging (ISBI);2014:53–56. https://doi.org/10.1109/ISBI.2014.6867807

[53] Al-Bander B, Williams B, Al-Nuaimy W, Al-Taee M , Pratt H, Zheng Y .Dense Fully Convolutional Segmentation of the Optic Disc and Cup in Colour Fundus for Glaucoma Diagnosis Symmetry 2018;10:87. https://doi.org/10.3390/sym10040087

[54] Haleem MS, Han L, van Hemert J, Li B. Automatic extraction of retinal features from colour retinal images for glaucoma diagnosis: a review. Comput Med Imaging Graph 2013:37:7–8:581–596.https://doi.org/10.1016/j.compmedimag.2013.09.005

[55] Abbas Q. Glaucoma-Deep: Detection of Glaucoma Eye Disease on Retinal Fundus Images using Deep Learning.International Journal of Advanced Computer Science and Applications 2017:8. https://doi.org/10.14569/IJACSA.2017.080606

[56] Thakur N, Juneja M.Survey on segmentation and classification approaches of optic cup and optic disc for diagnosis of glaucoma. Biomedical Signal Processing and Control 2018 :42;162–189. https://doi.org/10.1016/j.bspc.2018.01.014

[57] Mvoulana A, Kachouri R, Akil M.Fully automated method for glaucoma screening using robust optic nerve head detection and unsupervised segmentation based cup-to-disc ratio computation in retinal fundus images. Computerized Medical Imaging and Graphics 2019:77;p. 101643. https://doi.org/10.1016/j.compmedimag.2019.101643

[58] Karmawat R, Gour N, Khanna P .Glaucoma Detection using Fuzzy C-means Optic Cup Segmentation and Feature Classification.In: 2019 IEEE Conference on Information and Communication Technology;2019: 1–5. https://doi.org/10.1109/CICT48419.2019.9066165

[59] Panda R , Puhan NB, Panda G .Mean curvature and texture constrained composite weighted random walk algorithm for optic disc segmentation towards glaucoma screening", Healthcare Technology Letters 2018; 5:31–37. https://doi.org/10.1049/htl.2017.0043

[60] Chakravarty A , Sivaswamy J.Glaucoma classification with a fusion of segmentation and image-based features. In: 2016 IEEE 13th International Symposium on Biomedical Imaging (ISBI);2016: 689–692. https://doi.org/10.1109/ISBI.2016.7493360

[61] Sharma A, Aggarwal M, Roy SD, Gupta V, Automatic Glaucoma Diagnosis in Digital Fundus images using Convolutional Neural Network, in: 2019 5th International Conference on Signal Processing, Computing and Control (ISPCC);2019: 160–165. https://doi.org/10.1109/ISPCC48220.2019.8988512

[62] Besenczi R, Szitha K, Harangi B, Csutak A, Hajdu A. Automatic optic disc and optic cup detection in retinal images acquired by mobile phone. in: 2015 9th International Symposium on Image and Signal Processing and Analysis (ISPA);2015: 193–198. https://doi.org/10.1109/ISPA.2015.7306057

[63] Zilly J, Buhmann JM, Mahapatra D.Glaucoma Detection Using Entropy Sampling And Ensemble Learning For Automatic Optic Cup And Disc Segmentation", Computerized Medical Imaging and Graphics.2017;55:28–41. https://doi.org/10.1016/j.compmedimag.2016.07.012

[64] Soorya M, Issac A, Dutta MK, An automated and robust image processing algorithm for glaucoma diagnosis from fundus images using novel blood vessel tracking and bend point detection, International Journal of Medical Informatics.2018;110:52–70. https://doi.org/10.1016/j.ijmedinf.2017.11.015

[65] Phasuk S, Tantibundhit C, Poopresert P , Yaemsuk, A , Suvannachart P., Itthipanichpong, R., et al .Automated Glaucoma Screening from Retinal Fundus Image Using Deep Learning .In :41st Annual International Conference of the IEEE Engineering in Medicine and Biology Society (EMBC);2019; 904–907.

[66] Cheng, J, YinF, Wong W, Tao D, Liu, J. Sparse Dissimilarity-Constrained Coding for Glaucoma Screening. IEEE transactions on bio-medical engineering 2015;62(05). https://doi.org/10.1109/TBME.2015.2389234

[67] Dagade HG,Chougule S,Kapse R.Driver Alertness Monitoring using OpenCV and Android Smartphone.In : International Conference on "Emerging Research trends in Applied Engineering and Technology 2016

[68] Juang J, Chen C-Y, YangC-F. Proceedings of the 2nd International Conference on Intelligent Technologies and Engineering Systems (ICITES2013), Lecture Notes in Electrical Engineering. Springer International Publishing 2014 , ISBN10 3319045725 , ISBN13 9783319045726

[69] ZhiYu Chen, Abidi, B. R., Page, D. L., & Abidi, M. A. (2006). Gray-level grouping (GLG): an automatic method for optimized image contrast Enhancement-part I: the basic method. IEEE Transactions on Image Processing, 15(8), 2290–2302.

[70] X. Chen, S. Li, & J. Hu. (2014). A survey on Otsu image segmentation methods. In Journal of Computational Information Systems.

[71] Suzuki, S., & be, K. (1985). Topological structural analysis of digitized binary images by border following. Computer Vision, Graphics, and Image Processing, 30(1), 32–46

[72] Madroñal, D., Lazcano, R., Salvador, R., Fabelo, H., Ortega, S., Callico, G. M., Sanz, C. (2017). SVM-based real-time hyperspectral image classifier on a manycore architecture. Journal of Systems Architecture, 80, 30–40.